gout, urate, and crystal deposition disease

MDPI

Article

Length of Monosodium Urate Crystals in Synovial Fluid Based on Ultrasound Articular Deposits: Advancements in Crystallization Process

Elena Sansano-Muñoz [1], María-del-Carmen López-González [2], Cristina Rodríguez-Alvear [3], Irene Calabuig [4], Agustín Martínez-Sanchis [4], Carlos Rodríguez-Navarro [5], Eliseo Pascual [6] and Mariano Andrés [4,6,*]

1 Radiology Department, Dr. Balmis General University Hospital, 03010 Alicante, Spain; elena.sansano@goumh.umh.es
2 Rheumatology Department, La Ribera University Hospital, 46600 Alzira, Spain; lopgon.maricarmen@gmail.com
3 Rheumatology Department, Virgen de la Peña General Hospital, 35600 Fuerteventura, Spain; rodriguezalvearcristina@gmail.com
4 Rheumatology Department, Alicante Institute for Health and Biomedical Research (ISABIAL), Dr. Balmis General University Hospital, 03010 Alicante, Spain; irecalasa@gmail.com (I.C.); martinez_agu@gva.es (A.M.-S.)
5 Department of Mineralogy and Petrology, University of Granada, 18012 Granada, Spain; carlosrn@ugr.es
6 Department of Clinical Medicine, Miguel Hernández University, 03550 Alicante, Spain; pascual_eli@gva.es
* Correspondence: mariano.andresc@umh.es

Abstract

Objective: Monosodium urate (MSU) crystallization in human joints is poorly understood. This study aimed to investigate whether the length of MSU crystals varies in relation to organized ultrasound deposits, which may lead to longer crystals. **Methods**: Observational, cross-sectional study analyzing MSU crystals from synovial fluid samples of patients with crystal-proven gout. Using light microscopy, we measured crystal lengths (in μm) and noted the presence of long crystals, defined by cutoffs at the 66th, 75th, and 90th percentiles. We evaluated their association with two ultrasound-defined crystal deposition models: (1) grade 2–3 double-contour (DC) sign, tophi, and/or aggregates; and (2) grade 2–3 DC sign and/or tophi. **Results**: In a total of 1076 MSU crystals from 28 joints, median length was 23.3 μm (95% confidence interval 22.1–24.5). MSU crystal length was similar regardless of ultrasound deposition: in model 1 (20 joints, 71.4%), 22.5 μm in joints with deposits vs. 21.7 μm without; $p = 0.42$; in model 2 (15 joints, 53.6%), 22.8 μm vs. 21.2 μm, respectively; $p = 0.12$. Joints fulfilling model 2 criteria had more long crystals (>66th percentile), both in absolute and relative terms. Long crystals mildly correlated with serum urate levels and were numerically more frequent in patients with tophaceous gout. **Conclusions**: Most MSU crystals in synovial fluid gathered around a common length, regardless of ultrasound deposition. Long crystals were more common in joints with DC signs or tophi. Our finding is in keeping with two different mechanisms of MSU crystallization in humans.

Keywords: gout; monosodium urate crystals; length; ultrasound; double-contour sign; tophi; crystallization

check for updates

Received: 9 May 2025
Revised: 10 October 2025
Accepted: 13 October 2025
Published: 3 November 2025

Citation: Sansano-Muñoz, E.; López-González, M.-d.-C.; Rodríguez-Alvear, C.; Calabuig, I.; Martínez-Sanchis, A.; Rodríguez-Navarro, C.; Pascual, E.; Andrés, M. Length of Monosodium Urate Crystals in Synovial Fluid Based on Ultrasound Articular Deposits: Advancements in Crystallization Process. *Gout Urate Cryst. Depos. Dis.* **2025**, *3*, 21. https://doi.org/10.3390/gucdd3040021

Copyright: © 2025 by the authors. Published by MDPI on behalf of the Gout, Hyperuricemia and Crystal Associated Disease Network. Licensee MDPI, Basel, Switzerland. This article is an open access article distributed under the terms and conditions of the Creative Commons Attribution (CC BY) license (https://creativecommons.org/licenses/by/4.0/).

1. Introduction

Gout is often regarded as a chronic disease despite being potentially reversible and curable following a targeted urate-lowering strategy. The disease is defined by monosodium

urate (MSU) crystal deposition in tissues, most commonly in joints. The native immune reaction against crystals leads to arthritis, with oscillating intensity of inflammation. The crystallization of soluble urate as MSU depends on the level of hyperuricemia, which usually persists for an undefined (but probably long) period, favoring the accumulation of crystals in soft tissues before becoming symptomatic [1]. Indeed, several reports evidence the presence of tophaceous deposits in patients suffering their first gout flare [2,3]. However, it is unclear why less than half of hyperuricemic patients, including some with MSU crystal deposition [4], go on to develop clinical gout [5,6]. Moreover, without proper management, the subsequent disease course varies widely in terms of crystal load and flare frequency. In this sense, understanding the mechanisms behind MSU crystallization and the inflammatory reaction to crystals would be helpful to understand transitions along disease stages and variations in gouty clinical phenotypes.

The formation and deposition of MSU crystals are key to gout pathogenesis [7]. However, MSU crystallization has received scant attention in the literature. Advancing our knowledge on MSU crystallization in humans would shed light on the transition among the different disease stages [8] and the implications of crystal growth [9], helping clinicians tailor strategies to attain effective and rapid MSU crystal dissolution [10]. The supersaturation of serum urate (>6.8 mg/dL) is a crucial step, and its degree is one determinant of the rate of crystal growth. Several reports suggest a crystallization promoter in gouty synovial fluid (SF) compared to degenerative and rheumatoid fluids [11–14]. A protein nature is suspected, as the effect is lost after thermal shock. Type I and II collagens have been shown to promote MSU crystallization [14,15], inflammasome activation [16], and cell infiltration [15]. Crystal deposition and gout flares are more common in lower limb joints, which bear body weight and are prone to osteoarthritis [17]. Damaged collagen in articular cartilage is found in the early stages of osteoarthritis [18]. Joints with trauma or surgical damage are also at risk of MSU crystal deposition. On the other hand, the role of some crystallization inhibitors, such as lubricin [19], remains to be elucidated. Other implicated factors in MSU crystallization are low temperature, acid pH, and low calcium levels [20]. This array of variables likely explains why the same urate concentration may lead to different gouty phenotypes. But it also suggests that the process of MSU crystallization might not be uniform among those phenotypes.

Crystal precipitation, or nucleation, is a rate-limiting step in crystal formation [11]. The molecules dispersed in the solution merge into clusters by overcoming the solvent dispersion forces and forming crystal nuclei. Nucleation can be homogeneous if the crystal forms without a foreign surface or heterogeneous if it occurs on a foreign surface (including proteins or another crystal). If new crystals form over preexisting ones, it is called secondary nucleation. The heterogeneous and secondary forms may require lower levels of urate. Using human gouty SF, our group demonstrated that MSU crystallization initiates from small, non-inflammatory amorphous precursors, leading to acicular MSU crystals that possess a biological imprint absent in synthetic MSU crystals. This finding aligns with heterogeneous nucleation from protein templates [21] and is consistent with the bands of fibers that are occasionally observed in SF, which exhibit deposited and organized MSU crystals under polarized light microscopy (PLM) [22,23]. Interestingly, all deposited crystals seemed to have a similar length, perhaps determined by the protein template. In parallel, frozen sections of tophi steadily showed highly organized crystals in a fan display [24]. Such fan-like structures are occasionally seen in SF samples [25], perhaps shedding from organized deposits formed in the synovium [2]. MSU crystals from these fan-like structures are apparently longer than usual crystals from SF. Greater length and high level of organization are suggestive of formation after other crystals. Hence, variations

in MSU crystal lengths might indicate the occurrence of a double crystallization mechanism in people with gout.

To add more data that support this hypothesis, we aimed to assess whether the length of MSU crystals and the presence of long crystals are associated with the presence and characteristics of urate deposits as detected by ultrasound in the index joint.

2. Methods

This observational, cross-sectional study included patients with gout, during either flares or intercritical periods, seen at the rheumatology section of a tertiary academic hospital. Eligible patients could come from wards, emergency departments, or outpatient clinics. Gout flare was considered in cases of evident, acute arthritis with demonstration of MSU crystals [26].

Inclusion criteria were: demonstration of MSU crystals under PLM by a trained rheumatologist; sufficient SF sample for testing (by consensus, at least 0.5 cc); available ultrasound scan of the affected joint at the time of examination; and signed informed consent. We excluded cases with calcium pyrophosphate (CPP) crystals on PLM, intra-articular infiltration with depot glucocorticoids in the previous four weeks, according to current triamcinolone and betamethasone summaries of product characteristics; and aspirated prosthetic joint.

Patients that fulfilled selection criteria and agreed to participate in the study were recruited consecutively.

2.1. Study Procedures

Two observers (ES and MDCLG) analyzed the SF samples, unaware of the samples' origin and clinical or ultrasound data. MDCLG was a final-year rheumatology resident who routinely used PLM in clinical practice. ES was a final-year medical student who first underwent brief, dedicated training in PLM and visualization of MSU crystals, learning to identify and differentiate them from CPP crystals. ES's reliability was tested against an expert observer (MA), with an agreement of Cohen's κ of 1.0 in crystal identification and 1.0 in differentiation between MSU and CPP, performed on 24 observations of three samples (one without crystals, one with MSU, and the other with CPP). ES and MDCLG demonstrated high inter-rater reliability ($\kappa = 1.0$, $p < 0.001$), simultaneously assessing 20 SF samples with a microscope equipped with two viewing seats.

SF samples were analyzed either fresh or after being stored at +4 °C for no more than seven days. In case of delayed analysis, fluids were placed in heparin-containing tubes to maximize crystal visualization [27]. At the time of analysis, a small drop was placed on a glass slide and spread across the slide with the rounded edge of another slide, to create a thin smear for improved crystal visualization. Subsequently, the slide was covered with a long coverslip, and the preparation rested for at least 15 min to allow cells and crystals to settle. The sample was systematically reviewed. MSU crystals were identified by means of PLM and then measured using ordinary light. Per protocol, the length of at least five crystals from four separate fields were measured. All crystals present in each field were measured.

Ultrasound scans of the index joint were performed right before joint aspiration and SF analysis. The performers were trained rheumatologists (AMS and MA) with expertise in crystal-arthritis ultrasound and good intra-rater (Cohen's κ from 0.65 to 0.75; $p < 0.001$) and inter-rater reliability ($\kappa = 0.66$; $p = 0.001$) in evaluating MSU crystal deposits and PD inflammation [28].

2.2. Variables

The primary outcome variable was the length of MSU crystals in μm, measured at 400× magnification on a microscope equipped with a display previously calibrated using a Neubauer counting chamber. To fully explore our hypothesis, we were also interested in studying the presence of long crystals. There is no formal definition of long crystals in the literature, so we decided to use all the lengths measured in the entire crystal sample to define possible thresholds at the 66th, 75th, and 90th percentiles (P66, P75, or P90). This approach allowed us to explore the presence of crystals with lengths greater than those cutoffs.

The primary explanatory variable was ultrasound evidence of MSU crystal deposition at the index joint. Following OMERACT definitions [29], we registered the presence of the DC sign, tophi, and aggregates, scored as 0 (absent), 1 (possible), 2 (defined but minimal), or 3 (defined and severe). We also noted the presence of a local power Doppler (PD) signal to reflect the intensity and extent of the inflammatory process. The PD signal was classified according to the EULAR-OMERACT ultrasound task force [30] as grade 0 (absent), grade 1 (single focus), grade 2 (multifocal or occupying <50% of the joint surface), or grade 3 (occupying ≥50% of the joint surface). Grade 1 or superior was considered a positive PD signal.

As secondary explanatory variables, we selected some characteristics that may be indirect indicators of participants' crystal load: age (in years), sex (male/female), gout characteristics (current subcutaneous tophi, median SU levels in the last 2 years, use of urate-lowering therapy [ULT] at the time of the study, and history of oligo-polyarticular gout flares), presence of chronic kidney disease (according to KDIGO [31]), and use of loop diuretics or thiazides. Secondary variables were collected by interview, physical examination, and review of participants' electronic health records at study enrolment.

2.3. Statistics

No previous studies have been performed with the same aims, precluding the calculation of a sample size. The authors agreed to study at least 20 joints and 400 crystals, though we finally evaluated 1076 crystals from 28 joints.

The primary outcome variable (crystal length) and some explanatory variables are described using medians and their interquartile ranges (IQR), as the data distribution was non-parametric according to the Kolmogorov–Smirnov test. Categorical variables are represented using absolute and relative frequencies. We estimated the 95% confidence interval (CI) for the length of MSU crystals and categorized them into percentiles (P66, P75, and P90) to define the presence of long crystals. Using the P66, P75, and P90 cutoffs, we described the presence of long crystals using absolute (number of long crystals per sample) and relative frequency (percentage of long crystals relative to the total number of crystals per sample).

We used two definitions to categorize the presence of ultrasound deposits at the index joint: model 1 includes definite (grade 2–3) DC signs, tophi, and/or aggregates; and model 2, definite (grade 2–3) DC signs and/or tophi, given the low diagnostic value for the aggregates as considered by OMERACT [32].

The association between crystal length, long crystal counts, and the presence of model 1 or model 2 ultrasound signs was tested using the Mann–Whitney U test. Comparisons with individual ultrasound lesions (categorized as grade 2–3 yes/no), positive PD signal, or participants' clinical and laboratory characteristics were conducted using the Mann–Whitney U test or Spearman correlation, as needed. Statistical analyses were performed with SPSS v25 (IBM, Armonk, NY, USA) and Prism 9.4.1 (GraphPad Software, San Diego, CA, USA). The level of significance was set at $p < 0.050$.

The study was approved by the Alicante-Hospital General Ethics Committee [PI2022-119] and the Miguel Hernandez University of Elche Responsible Research Office [TFG.GME.ACM.SME.221111]. Participants were informed of the project aims, read and understood the information sheet, and provided written informed consent for participation.

3. Results

Study samples were obtained from 28 joints in 25 patients (three cases with oligoarticular flares). Two cases were included during the intercritical period, while the rest were enrolled during a flare. Participants' characteristics are presented in Table 1. They were predominantly middle-aged men experiencing a flare, mainly with knee involvement (50%). Over 30% presented subcutaneous tophi, and only one third were on ULT. Regarding ultrasound findings, model 1 and model 2 were met in 71.4% (n = 20) and 53.6% (n = 15) of studied joints, respectively. Eleven joints (39.3%) exhibited a positive PD signal.

Table 1. Characteristics of the study participants (28 joints in 25 subjects).

Age, in years, median (IQR)	60.0 (54.0–72.3)
Males	26 (92.9)
2-years serum urate, in mg/dL, median (IQR) [**n** = 27]	7.5 (7.1–8.9)
Index joint	
Knee	14 (50.0)
MTP1	6 (21.4)
Ankle	5 (17.9)
Wrist	1 (3.6)
Others	2 (7.2)
Disease state at enrolment	
Flare	26 (92.9)
Intercritical period	2 (7.1)
Subcutaneous tophi	9 (32.1)
Prior oligo-polyarticular flares	12 (42.9)
Chronic kidney disease	8 (28.6)
Use of diuretics	11 (39.3)
Use of urate-lowering therapy	8 (28.6)
Ultrasound findings	
Double-contour sign	
Grade 0	15 (53.6)
Grade 1	5 (17.9)
Grade 2	5 (17.9)
Grade 3	3 (10.7)
Tophi	
Grade 0	16 (57.1)
Grade 1	1 (3.6)
Grade 2	6 (21.4)
Grade 3	5 (17.9)

Table 1. *Cont.*

Aggregates	
Grade 0	15 (53.6)
Grade 1	3 (10.7)
Grade 2	6 (21.4)
Grade 3	4 (14.3)
Model 1	20 (71.4)
Model 2	15 (53.6)
Power Doppler signal	
Grade 0	17 (60.7)
Grade 1	7 (25.0)
Grade 2	2 (7.1)
Grade 3	2 (7.1)

Data presented as n (%) unless stated otherwise. IQR: interquartile range. Model-1 accounts for grade 2–3 double contour sign, tophi, and/or aggregates. Model-2 accounts for grade 2–3 double contour sign and/or tophi.

Under the microscope, a total of 1076 crystals were measured. A median of 40.5 crystals (IQR 19.5–55.5) were analyzed per sample, with a delay from arthrocentesis to PLM of 0.5 days (0.0–1.1 days). The median crystal length was 23.3 μm (95%CI 22.1–24.5) (Figure 1). Lengths ranged from 4.2 μm to 167.4 μm. In the complete samples, P66 denoted a length of 30.7 μm, P75 36.0 μm, and P90 53.0 μm. Accordingly, the number of P66, P75, and P90 long crystals per sample was 10.0 (3.0–20.3 crystals), 4.5 (1.0–14.5 crystals), and 1.0 (0.0–5.0 crystals), respectively. Based on crystals per sample, the percentage of P66, P75, and P90 long crystals was 26.6% (11.1–38.8%), 16.3% (3.3–24.7%), and 1.8% (0.0–8.4%), respectively.

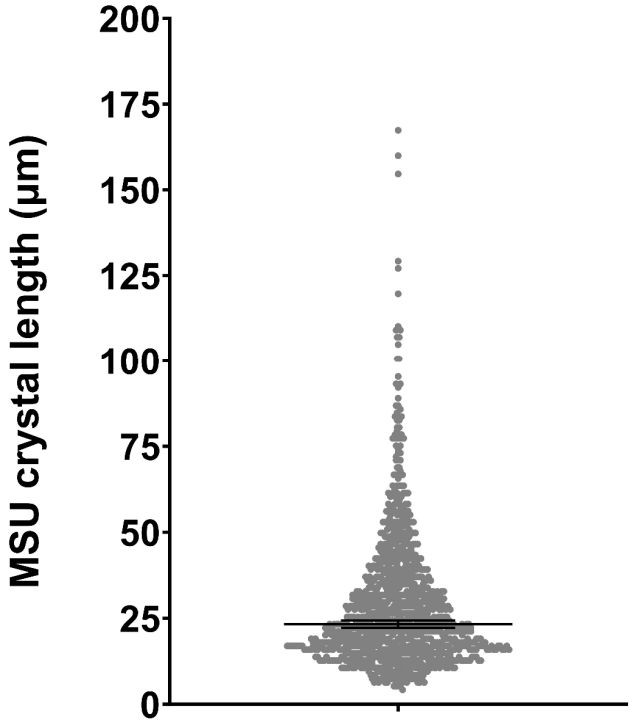


Figure 1. Distribution of monosodium urate crystal lengths across the entire sample. Bars indicate the median along with 95% confidence intervals.

3.1. Crystal Length and Long Crystals According to Ultrasound Model 1

Figure 2 compares the length of MSU crystals in joints that met model 1 criteria for ultrasound deposition (22.5 μm) versus those that did not (21.7 μm). A wider dispersion is observed in those with ultrasound deposits, but the difference was not statistically significant ($p = 0.42$).

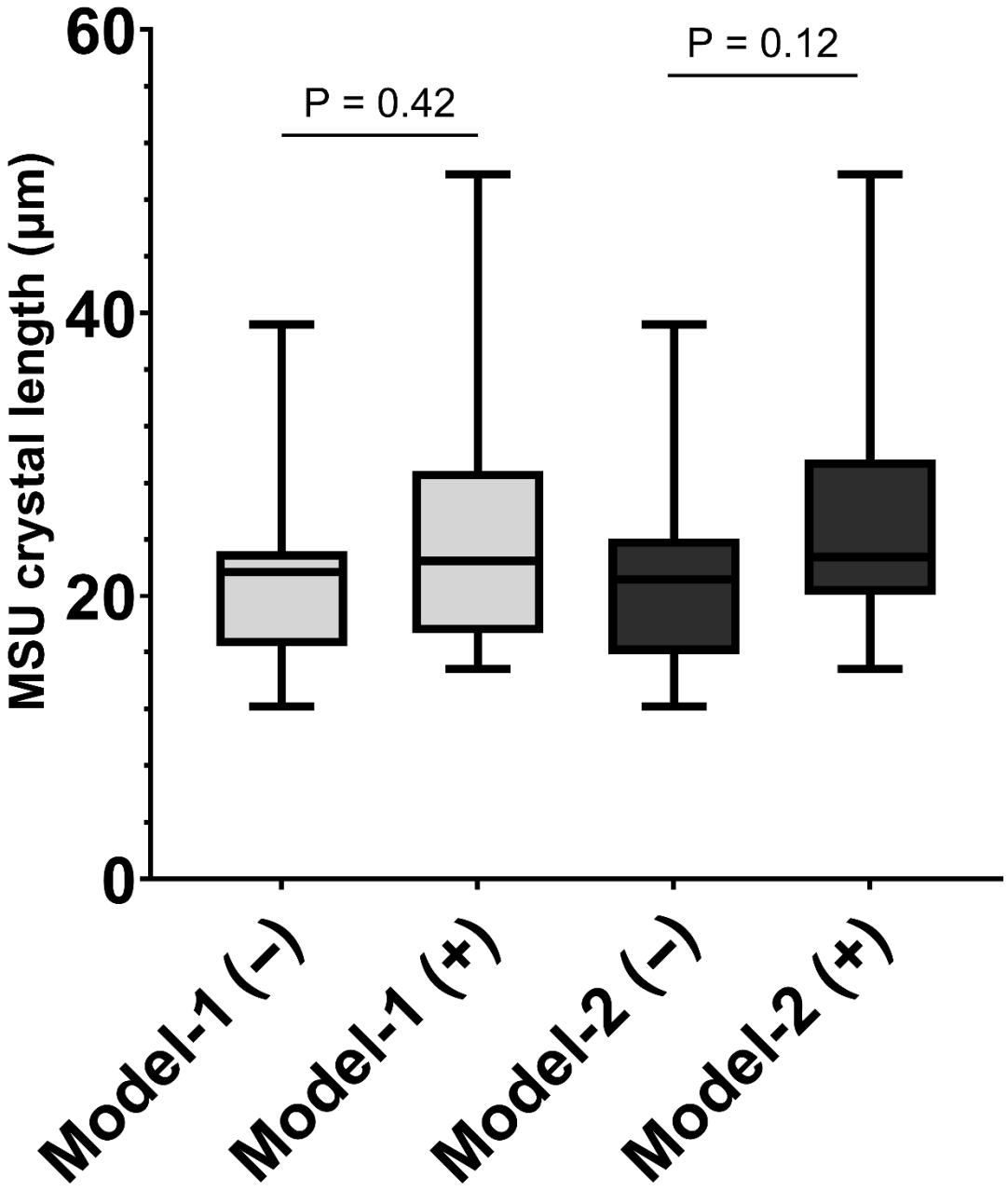


Figure 2. Box and whisker plot illustrating the lengths of monosodium urate (MSU) crystals considering the presence of ultrasound deposits, following Model-1 (grade 2–3 double contour sign, tophi, and/or aggregates, in light grey) or Model-2 (grade 2–3 double contour sign and/or tophi, in dark grey) definitions.

Regarding the presence of long crystals, no significant differences were observed in absolute numbers (Figure 3) or percentages of the total crystals (Figure 4).

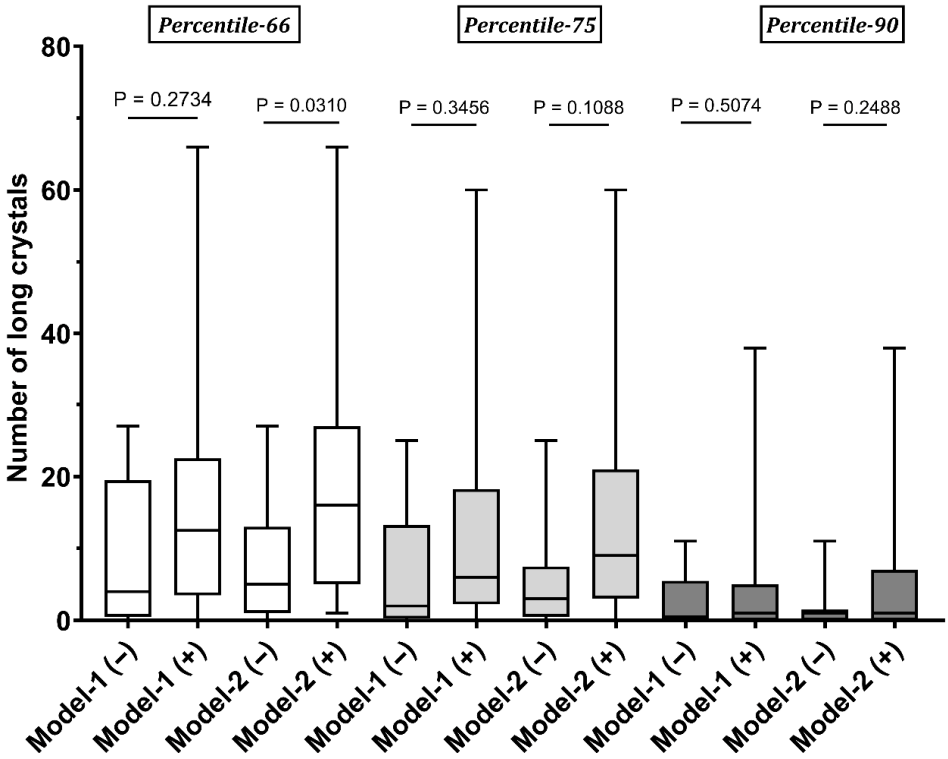


Figure 3. Comparison of the absolute number of long crystals based on the fulfillment of ultrasound Model-1 or Model-2. As shown, long crystals are categorized according to percentiles 66 (in white), 75 (in light grey), or 90 (in dark grey).

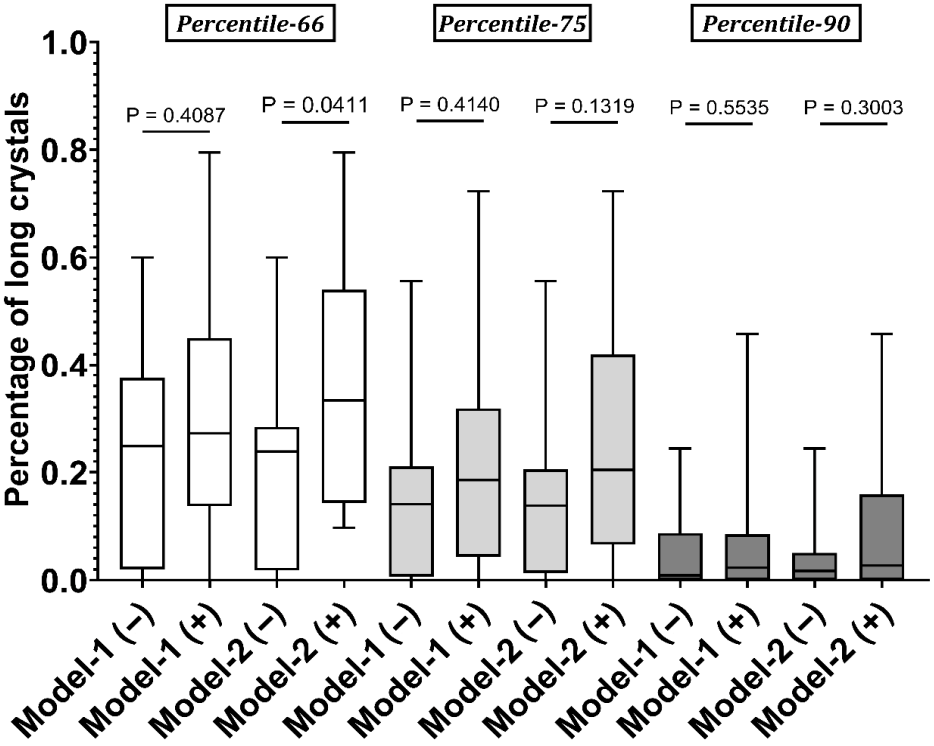


Figure 4. Comparison of the percentage of long crystals relative to the total number of MSU crystals based on the fulfillment of ultrasound Model-1 or Model-2. As shown, long crystals are categorized according to percentiles 66 (in white), 75 (in light grey), or 90 (in dark grey).

3.2. Crystal Length and Long Crystals According to Ultrasound Model 2 (DC Sign and Tophi as Organized Deposits)

Crystal length in joints that met model 2 criteria was similar to those without organized deposits (22.78 µm vs. 21.19 µm, $p = 0.12$) (Figure 2). Interestingly, the absolute and relative number of long MSU crystals according to the P66 threshold was significantly greater in model 2(+) joints (Figures 3 and 4). The difference in long crystals classified using the P75 and P90 definitions did not reach statistical significance.

3.3. Comparisons of Individual Ultrasound Features and Clinical and Laboratory Characteristics

No significant associations were found with individual ultrasound deposits, except that long crystals were more common in joints with a grade 2–3 DC sign (Table 2). A positive PD signal in the assessed joint was not associated with crystal length or long crystals.

Table 2. Comparative analysis of MSU crystal length, the number of large crystals, and individual ultrasound features in the assessed joint.

	G2–3 DC Sign			G2–3 Tophi			G2–3 Aggregates			(+) Power Doppler Signal		
	No	**Yes**	***p***	**No**	**Yes**	***p***	**No**	**Yes**	***p***	**No**	**Yes**	***p***
Crystal length, in µm	21.7 (16.9–25.3)	24.1 (21.5–29.7)	0.237	22.3 (16.9–25.2)	22.3 (16.9–32.3)	0.430	21.7 (16.9–23.8)	25.2 (17.9–33.2)	0.245	22.8 (18.3–27.5)	21.2 (15.9–26.5)	0.404
# of long crystals-P66	5.0 (2.0–16.8)	16.0 (7.3–29.3)	0.055	5.0 (2.0–17.0)	14.0 (3.0–27.0)	0.225	5.0 (2.8–18.8)	12.5 (4.3–27.0)	0.408	11.0 (3.0–24.0)	5.0 (2.0–17.0)	0.547
% of long crystals-P66	24.8 (8.7–32.5)	34.2 (25.5–52.6)	0.079	26.3 (5.8–33.3)	33.3 (13.5–54.5)	0.244	24.8 (10.2–35.0)	30.1 (16.2–59.3)	0.382	30.0 (15.4–44.2)	22.9 (9.7–33.3)	0.329
# of long crystals-P75	3.5 (0.3–12.0)	10.0 (3.3–21.0)	0.123	4.0 (1.0–10.0)	9.0 (1.0–21.0)	0.378	3.0 (0.8–12.0)	8.0 (3.5–21.8)	0.160	7.0 (1.0–18.0)	4.0 (1.0–13.0)	0.578
% of long crystals-P75	14.0 (6.8–21.3)	21.4 (9.9–40.0)	0.123	15.5 (3.1–20.7)	22.5 (3.2–45.5)	0.378	14.0 (2.0–20.6)	21.8 (9.4–48.2)	0.121	20.0 (7.0–28.2)	8.1 (3.2–25.5)	0.487
# of long crystals-P90	1.0 (0.0–4.5)	1.0 (0.0–9.5)	0.746	1.0 (0.0–3.5)	1.0 (0.0–11.0)	0.404	1.0 (0.0–5.0)	1.5 (0.0–12.3)	0.286	1.0 (0.0–6.0)	1.0 (0.0–5.0)	0.677
% of long crystals-P90	2.2 (0.0–7.9)	1.7 (0.0–18.5)	0.901	1.8 (0.0–6.7)	2.7 (0.0–22.0)	0.458	1.7 (0.0–8.2)	4.9 (0.0–27.6)	0.286	1.7 (0.0–9.0)	2.7 (0.0–8.6)	0.643

Data shown as median (IQR). G2–3: grade 2–3. P66: percentile 66. P75: percentile 75. P90: percentile 90.

A mild positive correlation was noted between average serum urate levels and the presence of long crystals (Table 3). The presence of P66 long crystals was numerically more common in patients with tophaceous gout. No associations were found with other clinical factors [Supplementary Material, Tables S1 and S2]. Sex and disease status (flare or intercritical) could not be analyzed, as only two participants were women or were included during the intercritical period.

Table 3. Correlations between average serum urate levels and the length of MSU crystals.

	2-Year Serum Urate	
	Rho	***p***
Crystal length	+0.26	0.184
# of long crystals-P66	+0.35	0.076
% of long crystals-P66	+0.36	0.065
# of long crystals-P75	+0.36	0.068

Table 3. *Cont.*

	2-Year Serum Urate	
	Rho	***p***
% of long crystals-P75	+0.37	0.061
# of long crystals-P90	+0.30	0.129
% of long crystals-P90	+0.29	0.134

P66: percentile 66. P75: percentile 75. P90: percentile 90.

4. Discussion

This is the first study evaluating whether the length of MSU crystals in SF may vary according to the presence of ultrasound crystal deposits in patients with gout. Overall, most MSU crystals were of a similar length (around 20 μm), regardless of ultrasound deposits. Sharing a common length would suggest that most crystals are formed using the same templates (probably proteins, such as collagen, as prior research has proposed [14–16]). In addition, we observed that the presence of long crystals (defined at P66) was more common in joints with organized deposits (DC signs or tophi). These long crystals resembled those seen in tophi sections [23,31]. This finding indicates that some MSU crystals might form over previously deposited crystals without using protein templates, suggesting secondary heterogeneous nucleation [23]. The phenomenon appears to be primarily local and unrelated to disease or laboratory characteristics, although an association was suggested with higher cumulative serum urate levels and tophaceous disease. Thus, it is likely that two different mechanisms of crystallization occur in people with hyperuricemia or gout.

MSU crystals from human samples or synthesized in a biological medium (sera or SF) show lengths of around 20–30 μm [33,34], as we also found in our study. Conversely, notably longer crystals are obtained if synthesized in abiotic media [35,36], where very high urate concentrations (over 30 mg/dL) are required for in vitro nucleation [37]. Available data suggest that MSU crystallization in SF begins with the amorphous precursor and progresses to short crystals through heterogeneous nucleation on a protein template, possibly detached from damaged or fibrillating collagen [38]. The process seems to be slow. If favorable physicochemical conditions persist, new crystals form through secondary nucleation in an organized manner and achieve greater lengths, likely due to lower supersaturation. Additionally, an Ostwald's ripening phenomenon might occur in the SF [39], where smaller crystals and more soluble amorphous MSU can dissolve and release ions that promote the growth of larger MSU crystals in organized deposits, such as tophi. Ostwald's ripening phenomenon possibly also explains long synthetic crystals in vitro. Understanding this process would help explain why tophi can form before the first flare [2,3] and could inform the development of strategies to prevent crystallization in asymptomatic hyperuricemia. A relationship between the length of MSU crystals and their inflammatory potential has been established in vitro and in vivo. Small and medium-sized crystals (from about 13 μm up to 23 μm) are the most effective in inducing IL-1β production [16,40,41]. In contrast, very large or very small ones are less flogistic. Thus, crystals in tophi—larger than those in SF—could potentially be less flogistic; this might explain why acutely inflamed tophi are uncommon in clinical practice. Further research is merited to understand whether flare recurrence in people with gout depends on crystal length, and if flare prophylaxis should be tailored accordingly.

The process of crystallization requires energy. The presence of longer crystals in joints with organized deposits might indicate that the nucleation and subsequent crystal growth would be easier, requiring overcoming a lower energy barrier, as they form heterogeneously on another crystal surface. In this case, an optimal self-epitaxial relationship among

MSU crystals would exist, typically resulting in a preferred crystallographic orientation, as commonly observed in tophi. Accordingly, those organized deposits would show an expansive growth that could be implicated in developing bone erosions. Imaging reports demonstrate that bone erosions in gout are intimately related to tophi [42–45], developed by local crystal growth and paracrine production of cytokines favoring osteoclast activation and osteoblast inhibition [9]. However, osteophytes and joint space reduction are not associated with local tophi. Moreover, treatment strategies focused on MSU crystal dissolution could help to ameliorate or prevent further damage [46]. Using rigorous urate targets for individuals with gout and organized crystal deposits also seems warranted [47,48].

We explored the use of two definitions to establish the presence of ultrasound crystal deposits in the index joint. Alongside DC sign and tophi, model 1 included aggregates since they are one of the most common ultrasound lesions in patients with gout [49] and tend to decrease during ULT [50]. However, similar signs may be observed in patients with CPP crystal disease, other inflammatory arthritis, and healthy individuals [51]. Furthermore, the pathological nature of aggregates remains uncertain. OMERACT advises against diagnosing gout solely based on aggregates, considering that an additional ultrasound element (DC sign or tophi) is necessary [32,52]. Despite aiming to study MSU crystallization, our findings align with this approach. Requiring DC sign or tophi (model 2) facilitated better discrimination of the presence of long crystals. This experience supports the lower specificity of aggregates and their weaker relationship with the body crystal load [53] and possibly with secondary nucleation.

We found no strong relationship between crystal length and most disease characteristics. However, long crystals showed a mild positive correlation with average serum urate levels and tophaceous gout. Both variables are indirect markers of high MSU crystal burden and correlate with ultrasound deposits [50,54]. Nevertheless, imaging studies indicate that the crystal deposition is already extensive in the early stages of the disease [55–57], even during asymptomatic hyperuricemia [58]. Thus, clinical characteristics likely play a limited role in predicting organized crystal deposition in the affected joint. We also studied the use of ULT at enrolment, which may shorten crystal length by promoting its dissolution from SF [59] and reducing tophi [60]. Nevertheless, we found no differences based on ULT, possibly because most patients exhibited hyperuricemia despite its use, which limited dissolution capability [61].

Overall, the homogeneous size and relatively narrow size distribution of MSU crystals identified in this study provides valuable information on MSU crystallization. A well-defined and narrow size distribution of crystals is typical of a biologically controlled biomineralization process, as is the case of bone apatite [62], aragonite in nacre [63], the cross-lamellar structure of mollusk shells [64], and calcite in eggshells [65]. Previous studies have shown that human MSU crystals show distinctive structural/textural features that point to a biologically controlled formation mechanism [21,24,66]. Such features are shared with various biominerals (from bone to mollusk shells or sea urchin spicules) [62,67,68]. One key feature is the recently observed formation of MSU after an amorphous precursor [21], which is general for other biominerals [69]. Moreover, in tophi, MSU crystals have been shown to arrange in a preferred crystallographic orientation (i.e., with parallel c-axes) [21], a tenet of biologically controlled biomineralization in eukaryote [70] that has also been observed in MSU crystals associated with collagen fibers in gout patients [23]. All these structural and textural features are controlled/regulated by a range of biomacromolecules (e.g., proteins) that control the nucleation and growth of such biominerals in an enclosed, privileged space [71]. While other biominerals provide functional benefits for an organism, in the case of pathological biomineralization of MSU, the effect is highly detrimental. Yet, it is very likely that the same mechanisms regulating the formation of other biominerals

(i.e., control by macromolecules) also operate in the pathological biomineralization of MSU in humans.

Among the strengths of our study were the large number of crystals studied. The analysts demonstrated excellent reliability in crystal detection at PLM despite being learners. We acknowledge that no formal comparison was tested for length measurement, as we used a simple procedure. The influence of sample storage in repeated crystal length measurement needs to be assessed further. However, SF observations were predominantly conducted with a short delay (less than 1 day). The crystals and ultrasound assessments were performed separately, and validated definitions of ultrasound deposits were used to establish their presence in the index joint. However, the techniques might overlook lesions (especially tophi) in less accessible joint areas, particularly in the knee. Over 1000 crystals were assessed, but only 28 joints were included, which may be inadequate for achieving statistical significance, particularly when comparing clinical characteristics or individual ultrasound lesions. Also, various lesions can manifest in a single joint, so identifying which lesion contributes to the assessed crystals is challenging. There were few female participants and intercritical gout cases, which should be a focus in future projects. There is no standard definition for long MSU crystals, so we evaluated three definitions based on the sample's percentiles. This approach needs further validation. Patients were recruited consecutively at rheumatology clinics and wards, which increased the likelihood of enrolling severe cases and hindered the ability to extrapolate findings to primary care or community settings.

In summary, most MSU crystals showed a similar average length (~20 μm) regardless of ultrasound deposits. However, joints with DC sign or tophi identified by ultrasound more commonly showed long crystals (length above the P66). No significant differences were observed when using P75 or P90 as the threshold for long crystals. Our findings might suggest the existence of two distinct mechanisms for MSU crystallization in human joints: one that deposits over fibers using protein templates and another in which an existing crystal serves as the foundation for the new crystal. Understanding MSU crystallization in humans may aid in developing targeted strategies for optimized dissolution and preventing its formation.

Supplementary Materials: The following supporting information can be downloaded at: https://www.mdpi.com/article/10.3390/gucdd3040021/s1, Table S1. Correlations between the age of participants and the length of MSU crystals. Table S2. Comparative analysis between MSU crystal length, number of long crystals, and participants' clinical characteristics.

Author Contributions: E.P. conceptualized the project; E.S.-M. and M.A. designed the study; M.-d.-C.L.-G., C.R.-A. and I.C. recruited participants; A.M.-S. and M.A. performed the ultrasound assessments; E.S.-M. and M.-d.-C.L.-G. performed the microscopy studies; E.S.-M., C.R.-N., E.P. and M.A. discussed and interpreted the results; E.S.-M. wrote the first draft of the manuscript; All authors have read and agreed to the published version of the manuscript.

Funding: The present project received no funding. The cost of manuscript edition and publication was covered by a research grant from Grunenthal (ref. CPRESA00091).

Institutional Review Board Statement: The study was conducted in accordance with the Declaration of Helsinki, and approved by the Alicante-General Hospital Health Department ethics committee (ref. PI2022-119, 26 October 2022) and the Miguel Hernandez University of Elche Responsible Research Office (ref. TFG.GME.ACM.SME.221111, 11 November 2022).

Informed Consent Statement: Informed consent was obtained from all subjects involved in the study.

Data Availability Statement: Data are available upon reasonable request from the researchers.

Acknowledgments: The authors thank Rocío Caño, and Silvia Gómez-Sabater, for their unvaluable research assistance.

Conflicts of Interest: M.A. has received advisory fees from Sobi and an ongoing research grant from Grunenthal. The other authors declare no conflicts of interest concerning the present research project.

References

1. Pineda, C.; Amezcua-Guerra, L.M.; Solano, C.; Rodriguez-Henríquez, P.; Hernández-Díaz, C.; Vargas, A.; Hofmann, F.; Gutiérrez, M. Joint and Tendon Subclinical Involvement Suggestive of Gouty Arthritis in Asymptomatic Hyperuricemia: An Ultrasound Controlled Study. *Arthritis Res. Ther.* **2011**, *13*, R4. [CrossRef] [PubMed]
2. Schumacher, H.R. Pathology of the Synovial Membrane in Gout. *Arthritis Rheum.* **1975**, *18*, 771–782. [CrossRef] [PubMed]
3. Bieber, A.; Schlesinger, N.; Fawaz, A.; Mader, R. Chronic Tophaceous Gout as the First Manifestation of Gout in Two Cases and a Review of the Literature. *Semin. Arthritis Rheum.* **2018**, *47*, 843–848. [CrossRef] [PubMed]
4. De Miguel, E.; Puig, J.G.; Castillo, C.; Peiteado, D.; Torres, R.J.; Martín-Mola, E. Diagnosis of Gout in Patients with Asymptomatic Hyperuricaemia: A Pilot Ultrasound Study. *Ann. Rheum. Dis.* **2012**, *71*, 157–158. [CrossRef]
5. Campion, E.W.; Glynn, R.J.; Delabry, L.O. Asymptomatic Hyperuricemia. Risks and Consequences in the Normative Aging Study. *Am. J. Med.* **1987**, *82*, 421–426. [CrossRef]
6. Dalbeth, N.; Phipps-Green, A.; Frampton, C.; Neogi, T.; Taylor, W.J.; Merriman, T.R. Relationship between Serum Urate Concentration and Clinically Evident Incident Gout: An Individual Participant Data Analysis. *Ann. Rheum. Dis.* **2018**, *77*, 1048–1052. [CrossRef]
7. Dalbeth, N.; Gosling, A.L.; Gaffo, A.; Abhishek, A. Gout. *Lancet* **2021**, *397*, 1843–1855. [CrossRef]
8. Dalbeth, N.; Stamp, L. Hyperuricaemia and Gout: Time for a New Staging System? *Ann. Rheum. Dis.* **2014**, *73*, 1598–1600. [CrossRef]
9. McQueen, F.M.; Chhana, A.; Dalbeth, N. Mechanisms of Joint Damage in Gout: Evidence from Cellular and Imaging Studies. *Nat. Rev. Rheumatol.* **2012**, *8*, 173–181. [CrossRef]
10. Pascual, E.; Andrés, M.; Vela, P. Gout Treatment: Should We Aim. for Rapid Crystal Dissolution? *Ann. Rheum. Dis.* **2013**, *72*, 635–637. [CrossRef]
11. Wilcox, W.R.; Khalaf, A.A. Nucleation of Monosodium Urate Crystals. *Ann. Rheum. Dis.* **1975**, *34*, 332–339. [CrossRef]
12. Tak, H.K.; Cooper, S.M.; Wilcox, W.R. Studies on the Nucleation of Monosodium Urate at 37 Degrees c. *Arthritis Rheum.* **1980**, *23*, 574–580. [CrossRef]
13. McGill, N.W.; Dieppe, P.A. Evidence for a Promoter of Urate Crystal Formation in Gouty Synovial Fluid. *Ann. Rheum. Dis.* **1991**, *50*, 558–561. [CrossRef] [PubMed]
14. McGill, N.W.; Dieppe, P.A. The Role of Serum and Synovial Fluid Components in the Promotion of Urate Crystal Formation. *J. Rheumatol.* **1991**, *18*, 1042–1045. [PubMed]
15. Xu, H.; Zhang, B.; Chen, Y.; Zeng, F.; Wang, W.; Chen, Z.; Cao, L.; Shi, J.; Chen, J.; Zhu, X.; et al. Type II Collagen Facilitates Gouty Arthritis by Regulating MSU Crystallisation and Inflammatory Cell Recruitment. *Ann. Rheum. Dis.* **2023**, *82*, 416–427. [CrossRef]
16. Chhana, A.; Pool, B.; Wei, Y.; Choi, A.; Gao, R.; Munro, J.; Cornish, J.; Dalbeth, N. Human Cartilage Homogenates Influence the Crystallization of Monosodium Urate and Inflammatory Response to Monosodium Urate Crystals: A Potential Link Between Osteoarthritis and Gout. *Arthritis Rheumatol.* **2019**, *71*, 2090–2099. [CrossRef]
17. Dalbeth, N.; Choi, H.K.; Joosten, L.A.B.; Khanna, P.P.; Matsuo, H.; Perez-Ruiz, F.; Stamp, L.K. Gout. *Nat. Rev. Dis. Primers* **2019**, *5*, 69. [CrossRef]
18. Chen, Y.-C.; Brown, C.P. Embrittlement of Collagen in Early-Stage Human Osteoarthritis. *J. Mech. Behav. Biomed. Mater.* **2020**, *104*, 103663. [CrossRef] [PubMed]
19. Elsaid, K.; Merriman, T.R.; Rossitto, L.-A.; Liu-Bryan, R.; Karsh, J.; Phipps-Green, A.; Jay, G.D.; Elsayed, S.; Qadri, M.; Miner, M.; et al. Amplification of Inflammation by Lubricin Deficiency Implicated in Incident, Erosive Gout Independent of Hyperuricemia. *Arthritis Rheumatol.* **2023**, *75*, 794–805. [CrossRef] [PubMed]
20. Martillo, M.A.; Nazzal, L.; Crittenden, D.B. The Crystallization of Monosodium Urate. *Curr. Rheumatol. Rep.* **2014**, *16*, 400. [CrossRef]
21. Rodriguez-Navarro, C.; Elert, K.; Ibañez-Velasco, A.; Monasterio-Guillot, L.; Andres, M.; Sivera, F.; Pascual, E.; Ruiz-Agudo, E. Unraveling the Pathological Biomineralization of Monosodium Urate Crystals in Gout Patients. *Commun. Biol.* **2024**, *7*, 828. [CrossRef]
22. Pascual, E.; Ordóñez, S. Orderly Arrayed Deposit of Urate Crystals in Gout Suggest Epitaxial Formation. *Ann. Rheum. Dis.* **1998**, *57*, 255. [CrossRef]
23. Pascual, E.; Martínez, A.; Ordóñez, S. Gout: The Mechanism of Urate Crystal Nucleation and Growth. A Hypothesis Based in Facts. *Jt. Bone Spine* **2013**, *80*, 1–4. [CrossRef]

24. Pascual, E.; Addadi, L.; Andrés, M.; Sivera, F. Mechanisms of Crystal Formation in Gout-a Structural Approach. *Nat. Rev. Rheumatol.* **2015**, *11*, 725–730. [CrossRef]
25. Fiechtner, J.J.; Simkin, P.A. Urate Spherulites in Gouty Synovia. *J. Am. Med. Assoc.* **1981**, *245*, 1533–1536. [CrossRef]
26. Bursill, D.; Taylor, W.J.; Terkeltaub, R.; Abhishek, A.; So, A.K.; Vargas-Santos, A.B.; Gaffo, A.L.; Rosenthal, A.; Tausche, A.-K.; Reginato, A.; et al. Gout, Hyperuricaemia and Crystal-Associated Disease Network (G-CAN) Consensus Statement Regarding Labels and Definitions of Disease States of Gout. *Ann. Rheum. Dis.* **2019**, *78*, 1592–1600. [CrossRef]
27. Pastor, S.; Bernal, J.-A.; Caño, R.; Gómez-Sabater, S.; Borras, F.; Andrés, M. Persistence of Crystals in Stored Synovial Fluid Samples. *J. Rheumatol.* **2020**, *47*, 1416–1423. [CrossRef]
28. Christiansen, S.N.; Filippou, G.; Scirè, C.A.; Balint, P.V.; Bruyn, G.A.; Dalbeth, N.; Dejaco, C.; Sedie, A.D.; Filippucci, E.; Hammer, H.B.; et al. Consensus-Based Semi-Quantitative Ultrasound Scoring System for Gout Lesions: Results of an OMERACT Delphi Process and Web-Reliability Exercise. *Semin. Arthritis Rheum.* **2021**, *51*, 644–649. [CrossRef]
29. D'Agostino, M.-A.; Terslev, L.; Aegerter, P.; Backhaus, M.; Balint, P.; Bruyn, G.A.; Filippucci, E.; Grassi, W.; Iagnocco, A.; Jousse-Joulin, S.; et al. Scoring Ultrasound Synovitis in Rheumatoid Arthritis: A EULAR-OMERACT Ultrasound Taskforce-Part 1: Definition and Development of a Standardised, Consensus-Based Scoring System. *RMD Open* **2017**, *3*, e000428. [CrossRef]
30. Calabuig, I.; Martínez-Sanchis, A.; Andrés, M. Sonographic Tophi and Inflammation Are Associated With Carotid Atheroma Plaques in Gout. *Front. Med.* **2021**, *8*, 795984. [CrossRef]
31. Lameire, N.H.; Levin, A.; Kellum, J.A.; Cheung, M.; Jadoul, M.; Winkelmayer, W.C.; Stevens, P.E.; Caskey, F.J.; Farmer, C.K.T.; Ferreiro Fuentes, A.; et al. Harmonizing Acute and Chronic Kidney Disease Definition and Classification: Report of a Kidney Disease: Improving Global Outcomes (KDIGO) Consensus Conference. *Kidney Int.* **2021**, *100*, 516–526. [CrossRef]
32. Terslev, L.; Gutierrez, M.; Schmidt, W.A.; Keen, H.I.; Filippucci, E.; Kane, D.; Thiele, R.; Kaeley, G.; Balint, P.; Mandl, P.; et al. Ultrasound as an Outcome Measure in Gout. A Validation Process by the OMERACT Ultrasound Working Group. *J. Rheumatol.* **2015**, *42*, 2177–2181. [CrossRef]
33. McGill, N.W.; Hayes, A.; Dieppe, P.A. Morphological Evidence for Biological Control of Urate Crystal Formation in Vivo and in Vitro. *Scand. J. Rheumatol.* **1992**, *21*, 215–219. [CrossRef]
34. Dieppe, P.; Swan, A. Identification of Crystals in Synovial Fluid. *Ann. Rheum. Dis.* **1999**, *58*, 261–263. [CrossRef]
35. Perrin, C.M.; Dobish, M.A.; Keuren, E.V.; Swift, J.A. Monosodium Urate Monohydrate Crystallization. *CrystEngComm* **2011**, *13*, 1111–1117. [CrossRef]
36. Yan, F.; Zhang, H.; Yuan, X.; Wang, X.; Li, M.; Fan, Y.; He, Y.; Jia, Z.; Han, L.; Liu, Z. Comparison of the Different Monosodium Urate Crystals in the Preparation Process and Pro-Inflammation. *Adv. Rheumatol.* **2023**, *63*, 39. [CrossRef]
37. Fiddis, R.W.; Vlachos, N.; Calvert, P.D. Studies of Urate Crystallisation in Relation to Gout. *Ann. Rheum. Dis.* **1983**, *42*, 12–15. [CrossRef]
38. Boyde, A. The Bone Cartilage Interface and Osteoarthritis. *Calcif. Tissue Int.* **2021**, *109*, 303–328. [CrossRef]
39. Ostwald, W.Z. Blocking of Ostwald Ripening Allowing Long-Term Stabilization. *Phys. Chem.* **1901**, *37*, 385.
40. Schumacher, H.R.; Fishbein, P.; Phelps, P.; Tse, R.; Krauser, R. Comparison of Sodium Urate and Calcium Pyrophosphate Crystal Phagocytosis by Polymorphonuclear Leukocytes. Effects of Crystal Size and Other Factors. *Arthritis Rheum.* **1975**, *18*, 783–792. [CrossRef]
41. Chhana, A.; Lee, G.; Dalbeth, N. Factors Influencing the Crystallization of Monosodium Urate: A Systematic Literature Review. *BMC Musculoskelet. Disord.* **2015**, *16*, 296. [CrossRef]
42. Dalbeth, N.; Clark, B.; Gregory, K.; Gamble, G.; Sheehan, T.; Doyle, A.; McQueen, F.M. Mechanisms of Bone Erosion in Gout: A Quantitative Analysis Using Plain Radiography and Computed Tomography. *Ann. Rheum. Dis.* **2009**, *68*, 1290–1295. [CrossRef] [PubMed]
43. Dalbeth, N.; Aati, O.; Kalluru, R.; Gamble, G.D.; Horne, A.; Doyle, A.J.; McQueen, F.M. Relationship between Structural Joint Damage and Urate Deposition in Gout: A Plain Radiography and Dual-Energy CT Study. *Ann. Rheum. Dis.* **2014**, *74*, 1030–1036. [CrossRef]
44. Pecherstorfer, C.; Simon, D.; Unbehend, S.; Ellmann, H.; Englbrecht, M.; Hartmann, F.; Figueiredo, C.; Hueber, A.; Haschka, J.; Kocijan, R.; et al. A Detailed Analysis of the Association between Urate Deposition and Erosions and Osteophytes in Gout. *ACR Open Rheumatol.* **2020**, *2*, 565–572. [CrossRef]
45. Wu, M.; Liu, F.J.; Chen, J.; Chen, L.; Wei, C.; Hu, Z.M.; Han, Y.; Lu, J.X.; Jiang, L.X.; Chen, H.B. Prevalence and Factors Associated With Bone Erosion in Patients With Gout. *Arthritis Care Res.* **2019**, *71*, 1653–1659. [CrossRef]
46. Dalbeth, N.; Billington, K.; Doyle, A.; Frampton, C.; Tan, P.; Aati, O.; Allan, J.; Drake, J.; Horne, A.; Stamp, L.K. Effects of Allopurinol Dose Escalation on Bone Erosion and Urate Volume in Gout: A Dual-Energy Computed Tomography Imaging Study Within a Randomized, Controlled Trial. *Arthritis Rheumatol.* **2019**, *71*, 1739–1746. [CrossRef]

47. Richette, P.; Doherty, M.; Pascual, E.; Barskova, V.; Becce, F.; Castañeda-Sanabria, J.; Coyfish, M.; Guillo, S.; Jansen, T.L.; Janssens, H.; et al. 2016 Updated EULAR Evidence-Based Recommendations for the Management of Gout. *Ann. Rheum. Dis.* **2017**, *76*, 29–42. [CrossRef]
48. Sivera, F.; Andrés, M.; Carmona, L.; Kydd, A.S.R.; Moi, J.; Seth, R.; Sriranganathan, M.; van Durme, C.; van Echteld, I.; Vinik, O.; et al. Multinational Evidence-Based Recommendations for the Diagnosis and Management of Gout: Integrating Systematic Literature Review and Expert Opinion of a Broad Panel of Rheumatologists in the 3e Initiative. *Ann. Rheum. Dis.* **2014**, *73*, 328–335. [CrossRef]
49. Naredo, E.; Uson, J.; Jiménez-Palop, M.; Martínez, A.; Vicente, E.; Brito, E.; Rodríguez, A.; Cornejo, F.J.; Castañeda, S.; Martínez, M.J.; et al. Ultrasound-Detected Musculoskeletal Urate Crystal Deposition: Which Joints and What Findings Should Be Assessed for Diagnosing Gout? *Ann. Rheum. Dis.* **2014**, *73*, 1522–1528. [CrossRef]
50. Hammer, H.B.; Karoliussen, L.; Terslev, L.; Haavardsholm, E.A.; Kvien, T.K.; Uhlig, T. Ultrasound Shows Rapid Reduction of Crystal Depositions during a Treat-to-Target Approach in Gout Patients: 12-Month Results from the NOR-Gout Study. *Ann. Rheum. Dis.* **2020**, *79*, 1500–1505. [CrossRef]
51. Chowalloor, P.V.; Keen, H.I. A Systematic Review of Ultrasonography in Gout and Asymptomatic Hyperuricaemia. *Ann. Rheum. Dis.* **2013**, *72*, 638–645. [CrossRef]
52. Christiansen, S.N.; Østergaard, M.; Slot, O.; Fana, V.; Terslev, L. Retrospective Longitudinal Assessment of Ultrasound Gout Lesions Using the OMERACT Semi-Quantitative Scoring System. *Rheumatology* **2022**, *61*, 4711–4721. [CrossRef]
53. Liu, E.; Dalbeth, N.; Pool, B.; Ramirez Cazares, A.; Ranganath, V.K.; FitzGerald, J.D. Ultrasound Findings of Monosodium Urate Aggregates in Patients with Gout. *Gout Urate Cryst. Depos. Dis.* **2023**, *1*, 83–88. [CrossRef]
54. de Ávila Fernandes, E.; Kubota, E.S.; Sandim, G.B.; Mitraud, S.A.V.; Ferrari, A.J.L.; Fernandes, A.R.C. Ultrasound Features of Tophi in Chronic Tophaceous Gout. *Skeletal Radiol.* **2011**, *40*, 309–315. [CrossRef]
55. Yokose, C.; Dalbeth, N.; Wei, J.; Nicolaou, S.; Simeone, F.J.; Baumgartner, S.; Fung, M.; Zhang, Y.; Choi, H.K. Radiologic Evidence of Symmetric and Polyarticular Monosodium Urate Crystal Deposition in Gout—A Cluster Pattern Analysis of Dual-Energy CT. *Semin. Arthritis Rheum.* **2020**, *50*, 54–58. [CrossRef]
56. Ottaviani, S.; Allard, A.; Bardin, T.; Richette, P. An Exploratory Ultrasound Study of Early Gout. *Clin. Exp. Rheumatol.* **2011**, *29*, 816–821.
57. Ogdie, A.; Taylor, W.J.; Neogi, T.; Fransen, J.; Jansen, T.L.; Schumacher, H.R.; Louthrenoo, W.; Vazquez-Mellado, J.; Eliseev, M.; McCarthy, G.; et al. Performance of Ultrasound in the Diagnosis of Gout in a Multicenter Study: Comparison With Monosodium Urate Monohydrate Crystal Analysis as the Gold Standard. *Arthritis Rheumatol.* **2017**, *69*, 429–438. [CrossRef] [PubMed]
58. Puig, J.G.; de Miguel, E.; Castillo, M.C.; Rocha, A.L.; Martínez, M.A.; Torres, R.J. Asymptomatic Hyperuricemia: Impact of Ultrasonography. *Nucleosides Nucleotides Nucleic Acids* **2008**, *27*, 592–595. [CrossRef] [PubMed]
59. Pascual, E.; Sivera, F. Time Required for Disappearance of Urate Crystals from Synovial Fluid after Successful Hypouricaemic Treatment Relates to the Duration of Gout. *Ann. Rheum. Dis.* **2007**, *66*, 1056–1058. [CrossRef]
60. Perez-Ruiz, F.; Calabozo, M.; Pijoan, J.I.; Herrero-Beites, A.M.; Ruibal, A. Effect of Urate-Lowering Therapy on the Velocity of Size Reduction of Tophi in Chronic Gout. *Arthritis Rheum.* **2002**, *47*, 356–360. [CrossRef]
61. Loeb, J.N. The Influence of Temperature on the Solubility of Monosodium Urate. *Arthritis Rheum.* **1972**, *15*, 189–192. [CrossRef] [PubMed]
62. Wopenka, B.; Pasteris, J.D. A Mineralogical Perspective on the Apatite in Bone. *Mater. Sci. Eng. C* **2005**, *25*, 131–143. [CrossRef]
63. Nudelman, F. Nacre Biomineralisation: A Review on the Mechanisms of Crystal Nucleation. *Semin. Cell Dev. Biol.* **2015**, *46*, 2–10. [CrossRef]
64. Rodriguez-Navarro, A.B.; Checa, A.; Willinger, M.-G.; Bolmaro, R.; Bonarski, J. Crystallographic Relationships in the Crossed Lamellar Microstructure of the Shell of the Gastropod Conus Marmoreus. *Acta Biomater.* **2012**, *8*, 830–835. [CrossRef]
65. Athanasiadou, D.; Jiang, W.; Goldbaum, D.; Saleem, A.; Basu, K.; Pacella, M.S.; Böhm, C.F.; Chromik, R.R.; Hincke, M.T.; Rodríguez-Navarro, A.B.; et al. Nanostructure, Osteopontin, and Mechanical Properties of Calcitic Avian Eggshell. *Sci. Adv.* **2018**, *4*, eaar3219. [CrossRef]
66. Paul, H.; Reginato, A.J.; Schumacher, H.R. Morphological Characteristics of Monosodium Urate: A Transmission Electron Microscopic Study of Intact Natural and Synthetic Crystals. *Ann. Rheum. Dis.* **1983**, *42*, 75–81. [CrossRef] [PubMed]
67. Addadi, L.; Joester, D.; Nudelman, F.; Weiner, S. Mollusk Shell Formation: A Source of New Concepts for Understanding Biomineralization Processes. *Chemistry* **2006**, *12*, 980–987. [CrossRef]
68. Seto, J.; Ma, Y.; Davis, S.A.; Meldrum, F.; Gourrier, A.; Kim, Y.-Y.; Schilde, U.; Sztucki, M.; Burghammer, M.; Maltsev, S.; et al. Structure-Property Relationships of a Biological Mesocrystal in the Adult Sea Urchin Spine. *Proc. Natl. Acad. Sci. USA* **2012**, *109*, 3699–3704. [CrossRef]
69. Addadi, L.; Raz, S.; Weiner, S. Taking Advantage of Disorder: Amorphous Calcium Carbonate and Its Roles in Biomineralization. *Adv. Mater.* **2003**, *15*, 959–970. [CrossRef]

70. Nudelman, F.; Sommerdijk, N.A.J.M. Biomineralization as an Inspiration for Materials Chemistry. *Angew. Chem. Int. Ed.* **2012**, *51*, 6582–6596. [CrossRef]
71. Gilbert, P.U.P.A.; Bergmann, K.D.; Boekelheide, N.; Tambutté, S.; Mass, T.; Marin, F.; Adkins, J.F.; Erez, J.; Gilbert, B.; Knutson, V.; et al. Biomineralization: Integrating Mechanism and Evolutionary History. *Sci. Adv.* **2022**, *8*, eabl9653. [CrossRef] [PubMed]

Disclaimer/Publisher's Note: The statements, opinions and data contained in all publications are solely those of the individual author(s) and contributor(s) and not of MDPI and/or the editor(s). MDPI and/or the editor(s) disclaim responsibility for any injury to people or property resulting from any ideas, methods, instructions or products referred to in the content.